International Journal of Pharmaceutics 606 (2021) 120923

Contents lists available at ScienceDirect

International Journal of Pharmaceutics

journal homepage: www.elsevier.com/locate/ijpharm

Self-stabilized Pt(IV) amphiphiles by precise regulation of branch length for enhanced chemotherapy

Xiao Kuang [a], Yuting Hu [a], Dongxu Chi [a], Haolin Zhang [a], Zhonggui He [a], Yiguo Jiang [b,*], Yongjun Wang [a,*]

[a] Department of Pharmaceutics, Wuya College of Innovation, Shenyang Pharmaceutical University, Shenyang 110016, China
[b] Department of Pharmacy, The Affiliated Suzhou Science & Technology Town Hospital of Nanjing Medical University, Suzhou 215153, China

ARTICLE INFO

Keywords:
Disulfide bond
Pt(IV) prodrug
Self-stabilization
Chemical modification
Antitumor performance

ABSTRACT

A surge of platinum(IV) compounds are utilized or investigated in cancer treatment but their therapeutic outcomes have been greatly compromised by remaining adverse effects and limited antitumor performance, attributable to nonspecific distribution and insufficient activation in tumor site. Herein, we designed a series of disulfide bond introduced Pt(IV)-lipid prodrugs with different branch length, all of which are able to self-stabilize into nanomedicine and be activated by high intracellular glutathione (GSH) level. The impact of precise modification of these prodrugs on their assembly stability, pharmacokinetics and cytotoxicity was probed to establish a connection between chemical structure and antiproliferation efficiency. With optimal assembly manner and delivery efficacy, the longest axial branched Pt(IV) prodrug CSS18 exhibited the most impressive therapeutic outcome, providing a potential path to more efficient nanocarriers for chemotherapeutic agents by chemical modulation and, giving insights into the rational design of reduction responsive platinum delivery system.

1. Introduction

Platinum(IV) complexes have aroused great interests in the field of chemotherapy for cancer treatment in the past few decades (Rottenberg et al., 2021; Wang and Lippard, 2005; Zajac et al., 2020; Wang et al., 2019). Compared with parent Pt(II) compounds, Pt(IV) prodrugs are more kinetically inert to ligand substitution before reduction, making it possible for platinum drugs to lower the rate of aquation and subsequent coordination with DNA inside cells. These unique properties make it possible for platinum candidates to improve their toxicology manners, which helps to attenuate side effects (Rabik and Dolan, 2007; Hartmann and Lipp, 2003; Pan et al., 2020). The alleviation of dose-limiting toxicity also increases patient tolerance and is expected to exert better antiproliferation efficacy against various tumor by virtue of elevated dosage of Pt drugs. However, the outcomes of Pt(IV) conjugates involved in clinical trials were far from satisfactory as none of them touched the final phase and entered the market. Most of them did not show enhanced antitumor efficiency over conventional Pt(II) drugs (cisplatin and carboplatin), presumably deriving from poor specific accumulation and insufficient DNA-crosslinked activity. Among them, satraplatin, the most successful oral Pt drug in clinical trials, with a better toxicity profile than cisplatin, showed impressive *in vitro* activity against cisplatin-resistant tumor cells (Doshi et al., 2012; Choy et al., 2008). Despite the relatively positive outcome of the Phase III trial, satraplatin still failed to obtain FDA approval for no significantly improved overall survival (Kelland, 2007). Selective tumor accumulation and activation are believed to be the pivotal factors of rationality designing Pt(IV) prodrugs to enable appreciable activity against malignancies.

Nanotechnology has been prevailing in application of drug delivery and regenerative medicine, endowing chemotherapeutics with good compliance, prolonged blood circulation and preferable accumulation in tumor (Shi et al., 2010; Luo et al., 2014), which seems to be capable of addressing the dilemma encountered by Pt(IV) prodrugs. Nonetheless, deficiency in drug loading capacity (DLC) and drawbacks originated from great utilization of excipients have greatly hindered the development of nanomedicine (Shi et al., 2010). Self-assembled prodrug nanocarriers take advantages of nanotech and achieve high DLC with minimum excipient employment, providing new insights into rational design of Pt delivery system. As previously investigated by us (Luo et al., 2014; Kuang et al., 2021; Wang et al., 2014), self-assembled

* Corresponding authors.
E-mail addresses: jiangyiguo0515@126.com (Y. Jiang), wangyongjun@syphu.edu.cn (Y. Wang).

https://doi.org/10.1016/j.ijpharm.2021.120923
Received 23 April 2021; Received in revised form 4 July 2021; Accepted 20 July 2021
Available online 23 July 2021

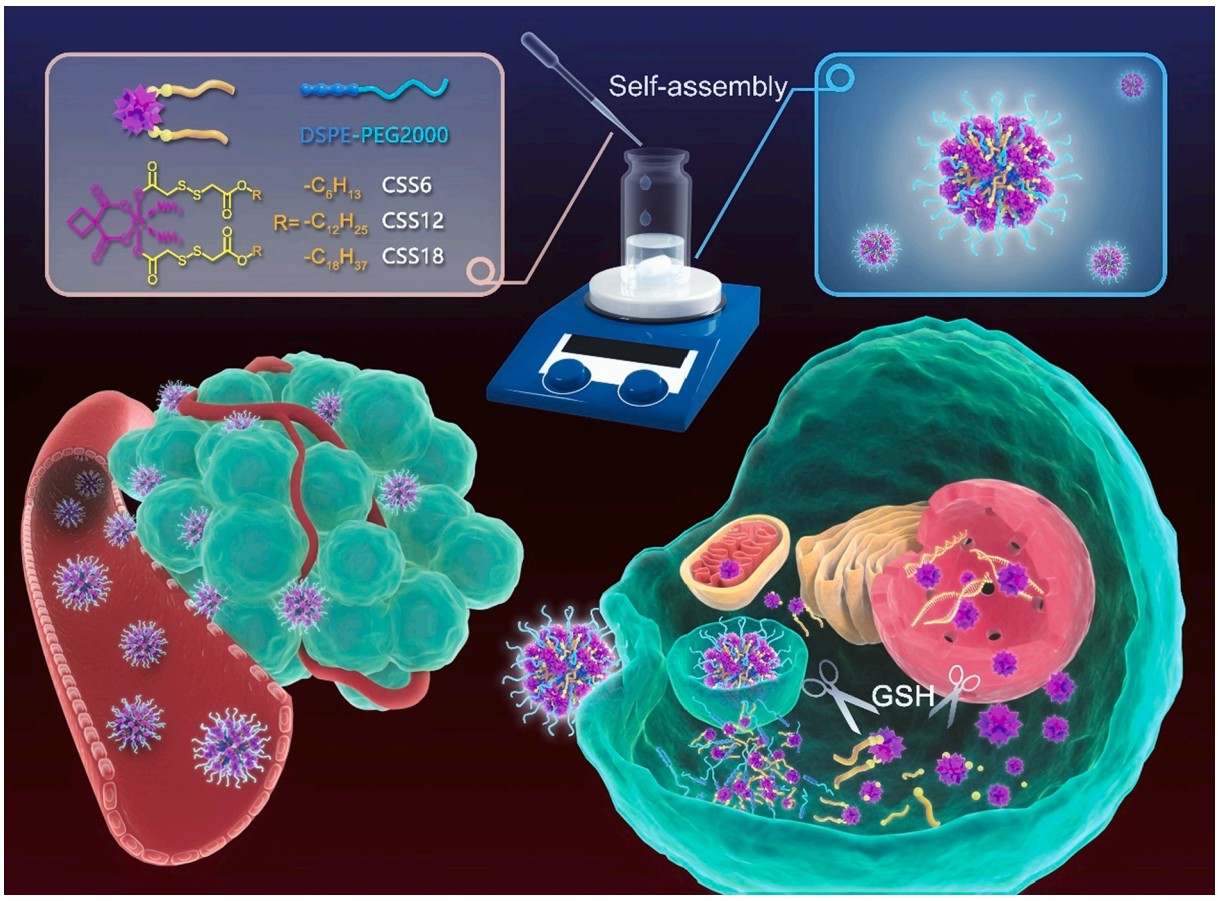

Fig. 1. Schematic illustration of self-stabilized Pt(IV) NPs for specific delivery of carboplatin and suppression of tumors. Disulfide introduced Pt(IV)-lipid prodrugs with different length of fatty tails can be activated by high intracellular GSH to enable antitumor performance of nanomedicine.

nanoparticles (NPs) are able to load much more therapeutic agents than other kinds of nanomedicine characterized with drug entrapment in hydrophobic cores, and some homodimeric prodrug nanoassemblies hit>65% of DLC (Yang et al., 2020; Zuo et al., 2020). The reported self-assembly mechanism of most prodrugs depend on π-π stacking dominated *van der Waals* interaction (Cheetham et al., 2017), for which it is challenging to design platinum-based assembled nanomedicine if no πe^- exists. Strong lipophobicity of platinum makes it difficult to construct stable Pt encapsulated nanocarriers due to precipitation tendency between heavy atoms (Rottenberg et al., 2021; Wang et al., 2019). Some Pt (IV)-lipid conjugates can transform into nanoparticles in aqueous solution but the procedure need the help of surfactants with large proportion (>60% w/w) (Chen et al., 2018; Ling et al., 2019) which is more like emulsification rather than self-assembly. The difficulty in preparation of Pt(IV) self-stabilized NPs impedes implement of high platinum loading capability. Stabilized and controllable assembly behavior is required for Pt(IV) NPs to enable enough tumor accumulation.

Insufficient activation is another drawback compromising therapeutic outcomes of Pt(IV) prodrugs. Stimulus responsive nanomedicine focus on the distinctive features of cancer cells or tumor microenvironment, augmenting activation on corresponding target and minimizing undesired effects in normal tissues. A typical product approved for sale is Mylotarg®, the first antibody-drug conjugate (ADC) on the market, covering a reduction responsive linker of disulfide bond (Damle and Frost, 2003). Disulfide cleavage is GSH-consuming and accelerated in cytoplasm where GSH level is 1000-fold higher than that of plasma (Schafer and Buettner, 2001; Brülisauer et al., 2014). The introduction of disulfide bond to specific prodrug has been proved a trigger for explosive drug release in tumor cells (Sun et al., 2018; Luo et al., 2016) but a harness of chemotherapeutics for prevention from leakage inside vessels (Lee et al., 2013). Selective activation in the targeted spot conducted by responsive bond may be one answer to addressing the discounted antitumor performance of Pt(IV) candidates (Reshetnikov et al., 2018; Yang et al., 2020).

Chemical structure of self-assembled prodrug exercises a decisive influence on assembly stability, consequent *in vivo* fate and resulting antiproliferation performance (Wang et al., 2015). The interactions between self-assembled nanomedicine and biocomponents such as proteins, phospholipid bilayers, nucleic acids and organelles, are necessary to be explored for awareness of drug disposal after administration. The colloidal chemistry of nanoparticles has a great impact on their destiny when encountering these biocomponents to form interfaces. Probing these interfaces promotes the predictive relationships between prodrug structure and therapeutic activity that are bridged by surface properties such as shape, size and outer coatings. For common nanomedicine, drug–carrier compatibility can be tuned by modifying carrier materials (Shi et al., 2015). It is simplified for self-assembled NPs here to focus on the rationality of prodrug design on the basis of physicochemical interaction. The "structure-assembly-activity" profile need to be established to endow self-assembled prodrug NPs with preferable drug accumulation and selective activation.

To deal with poor tumor accumulation and insufficient activation of Pt(IV) prodrugs, a series of disulfide bond introduced Pt(IV)-lipid amphiphiles with various branch length were prepared in this research. Carboplatin was chosen as model drug for relatively good water solubility (17 mg/mL) and carbon chains with different length as axial ligands to yield Pt(IV) amphiphiles (CSS6, CS12, CSS18, C-18 and mCSS18). These conjugates assembled stably in water with minimum PEGylation (15%) to produce uniform spherical NPs, namely self-stabilized Pt(IV) NPs, which rapidly disintegrated in high intracellular

GSH due to disulfide cleavage. (Fig. 1) The impacts of disulfide inserted branch length on assembly stabilization, pharmacokinetic manner and intracellular activation were probed to optimize drug–carrier compatibility for enhanced delivery efficacy. We found that the most hydrophobic conjugate of all, CSS18, exhibited the best self-stabilized capacity, highest tumor accumulation and consequent antitumor efficiency. Overall delivery benefits were ranked as: CSS18 > CSS12 > mCSS18 (equivalent to CSS9) > CSS6 that showed evident correlation to branch length. These results indicate a drug-carrier association that connect precise chemical constitution and delivery efficacy, providing insights into the rational design of Pt(IV) delivery system.

2. Materials and methods

2.1. Materials

Carboplatin (Car) was purchased from Meilun (Dalian, China). H_2O_2, 2,2′-disulfanediyldiacetic acid, acetic anhydride (Ac2O), adipic anhydride, 1-Hexanol, 1-Dodecanol and 1-Octadecanol were purchased from Aladdin (Shanghai, China). 1-Ethyl-3-(3-dimethylaminopropyl)-carbodiimide hydrochloride (EDCI) and 4-dimethylaminopyridine (DMAP) were obtained from Chemlin Pharm Co. Ltd. (Nanjing, China). DSPE-PEG_{2000} were obtained from AVT (Shanghai) Pharmaceutical Co., Ltd. Glutathione (GSH), GSH and GSSG assay kit were procured from Solarbio Science & Technology Co., Ltd (Beijing, China). ELISA kit and BCA protein assay kit was purchased from Neobioscience Technology Co, Ltd (Beijing, China).

2.2. Synthesis of Pt(IV) prodrugs

GSH-sensitive octahedrally coordinated carboplatin were synthesized by coupling oxidized carboplatin and aliphatic alcohol with disulfide linkage. 1-Hexanol, 1-Dodecanol and 1-Octadecanol were chosen as aliphatic branches of disulfide-linked Pt(IV) prodrugs (abbreviated as CSS6, CSS12, CSS18 respectively). And 1-Octadecanol was also grafted onto carboplatin with a hexanedioic acid-linkage to yield non-sensitive Pt(IV) prodrug (donated as C-18). Monocoordinated GSH-responsive carboplatin with 1-Octadecanol tethered was synthesized via similar method and described as mCSS18. Synthesis route and all experiment details were shown in support information. Chemical structures of all yield compounds were confirmed by MS (mass spectrum) and 1H NMR (nuclear magnetic resonance).

Briefly, CSS6, CSS12 and CSS18 were all prepared in a similar process. Briefly, 0.5 mmol Car(IV)–2OH was dispersed in 20 mL DMF at 35 °C with addition of DMF solution of 1.2 mmol 1,4,5-oxadithiepane-2,7-dione and 0.2 mmol DMAP, followed by continuous stirring for 12 h. Then 1 mmol EDCI was added to the reaction solution to activate carboxyl group for 20 min. And 1.5 mmol appropriate aliphatic alcohol (1-Hexanol, 1-Dodecanol or 1-Octadecanol) was added to the reaction mixture and the solution was stirred overnight. The resulting solution was filtered, evaporated to 2 mL, and added to 50 mL diethyl ether for precipitation. The deposition was collected, washed with diethyl ether, and dried under vacuum. The final products were weight for calculation of yields (CSS6: 56.1%, CSS12: 37.2% and CSS18: 40.3%). C-18 was synthesized by following procedures: 0.5 mmol Car(IV)–2OH was dispersed in 20 mL DMF at 40 °C with addition of DMF solution of 1.2 mmol adipic anhydride and 0.2 mmol DMAP, followed by continuous stirring for 12 h. Then 1 mmol EDCI was added to the reaction solution to activate carboxyl group for 20 min. And 1.4 mmol 1-Octadecanol was added to the reaction mixture and the solution was stirred overnight. The resulting solution was filtered, evaporated, and added to diethyl ether of large volume. The precipitate was collected, washed with diethyl ether, and dried under vacuum to yield pale yellow solid of C-18 (yield: 59.6%). mCSS18 was prepared in following process: 0.5 mmol Car(IV)–2OH was dispersed in 20 mL DMF at 35 °C with addition of DMF solution of 0.6 mmol 1,4,5-oxadithiepane-2,7-dione and 0.2 mmol DMAP, followed by continuous stirring for 12 h. Then 1 mmol EDCI was added to the reaction solution to activate carboxyl group for 20 min. And 0.8 mmol 1-Octadecanol was added to the reaction mixture and the solution was stirred overnight. The resulting solution was filtered, evaporated, and added to 50 mL diethyl ether. The precipitate was collected, washed with diethyl ether, and dried under vacuum. mCSS18 (yield: 55.2%).

2.3. Self-stabilization of Pt(IV) NPs

Moderate amount of Pt(IV) prodrug (CSS6, CSS12, CSS18, C-18 or mCSS18) were dispersed in 0.2 mL 0.35% DSPE-PEG_{2000} ethanol solution, followed by pipetting this mixture of prodrug and DSPE-PEG_{2000} dropwise to stirring deionized water with agitation of 600 rpm. Then residual ethanol of all formulations were removed through rotary evaporation under vacuum after 20 min agitation to yield self-stabilized Pt(IV) NPs. CSS6, CSS12, CSS18, C-18 and mCSS18 NPs at final equivalent Pt concentration of 0.5, 1.0, 1.5 mg/mL were prepared respectively and CSS18 NPs of 3 mg Pt/mL were also made with the same procedure. All Pt(IV) formulations were characterized by particle size, PDI and zeta potential with DLS. Typical photos of TEM were taken to indicate the morphology of NPs. And drug loading capacity was determined with inductively coupled plasma mass spectrometry (ICP-MS). Methods of sample preparation before measurement by ICP-MS were provided from Sci-Tech innovation Co. Ltd (Qingdao, China). We also evaluate the formation of colloid system via nanoprecipitation method in this process with a light beam passing through Pt(IV) NPs to confirm Tyndall effect.

2.4. Colloidal stability of Pt(IV) NPs

To probe the colloidal stability of all prodrug nanoparticles, 1 mL NPs sample was added to 20 mL PBS 7.4, containing 10% of fetal bovine serum (FBS). The mixtures were incubated at 37 °C with gentle shaking. At prescriptive intervals (0, 2, 4, 6, 8, 12, 24, 36, 48 h), the particle size was measured (n = 3 for each group). Meanwhile, 1 mL NPs was also added to 20 mL 10 mM PBS 7.4 and size of NPs were measured by Zetasizer (n = 3 for each group) within 7 days.

2.5. In vitro drug release

In vitro Pt release profile of various Pt(IV) NPs was investigated in 10 mM PBS 7.4 in presence of 1 mM and 10 mM GSH. Briefly, dialysis bag of MWCO 1000 D containing 1 mL Pt(IV) NPs was submerged into 20 mL release media which was placed under 37 °C and vibration at 100 rpm. At pre-programmed intervals, 1, 2, 4, 8, 12 and 24 h, 1 mL media was taken out to be analyzed by ICP-MS to quantify Pt content released from NPs.

2.6. Cell culture

Mouse breast cancer 4T1 cells, mouse melanoma B16-F10 cells, human ovarian carcinoma A2780 cells, and human fetal hepatocyte LO2 cells were obtained from Cell Resource Center, Shanghai Institutes for Biological Sciences, Chinese Academy of Sciences. 4T1, A2780 and LO2 cells were cultured in routine medium consisted of 90% RPMI 1640, 10% FBS. B16-F10 cells were cultured in routine medium consisted of 90% DMEM, 10% FBS, penicillin (30 mg/mL) and streptomycin (100 μg/mL). All cells were cultured at 37 °C in 5% CO_2 atmosphere.

2.7. Intracellular Pt accumulation

The level of cellular internalization was tested by treating 4T1 cells with Pt(IV) prodrugs and nanoparticles at equivalent concentration of 10 μg Pt/ml. Briefly, 4T1 cells were cultured in 12-well plates with a density of 1×10^5 cells/well for 24 h and then immersed with 10 μg Pt/

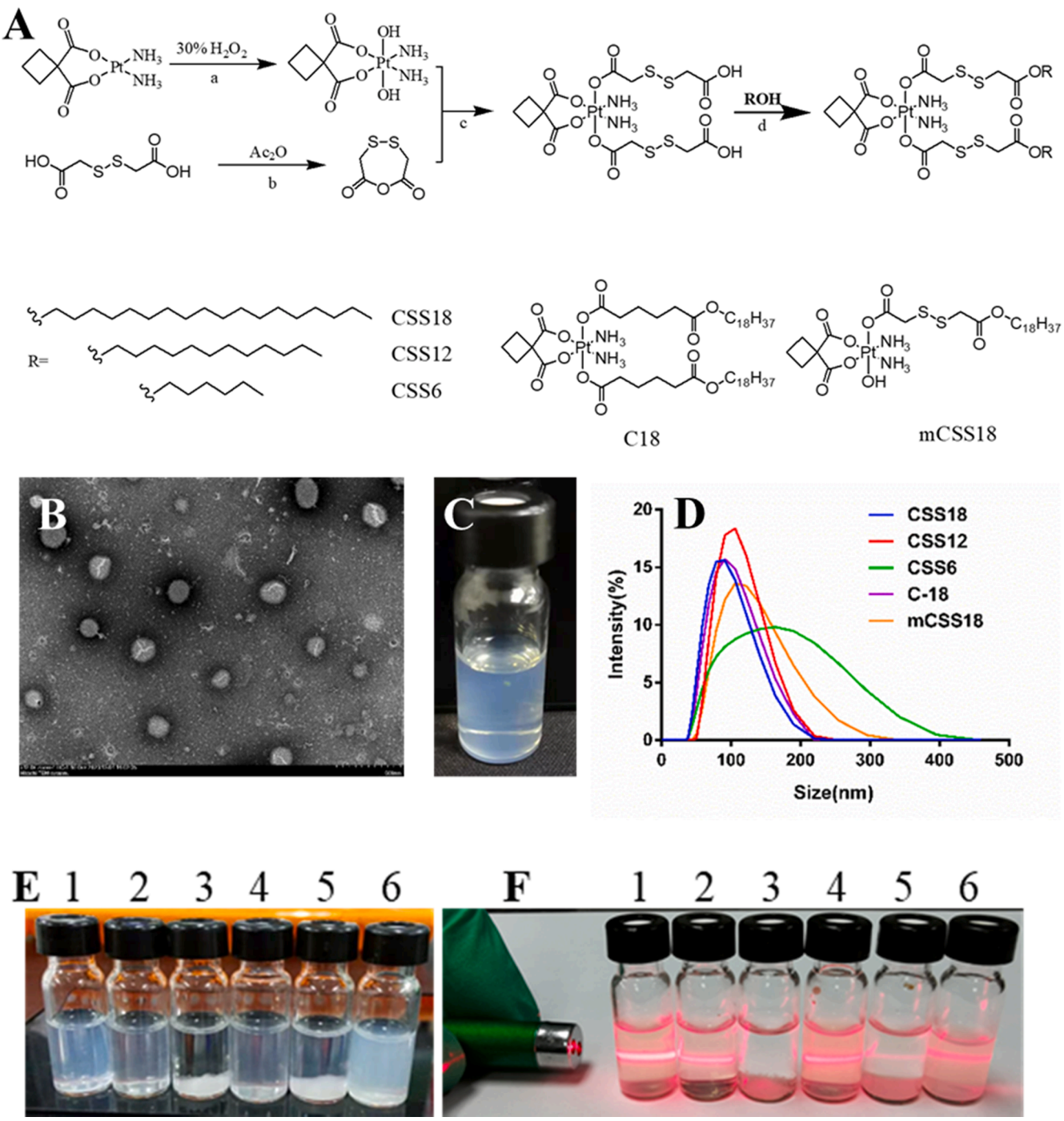

Fig. 2. (A) Synthesis route of disulfide bond bridged conjugate of carboplatin and different fatty chains. (a) 50 ℃, 3 h, H_2O; (b) 25 ℃, 2 h; (c) EDCI, DMAP, 45 ℃, 24 h, DMF; (d) EDCI, DMAP, 30 ℃, 12 h, DMF. (B) Typical TEM images of CSS18 NPs. Scale bar: 200 nm. (C) The appearance of CSS18 NPs at 1.5 mg Pt/mL. (D) Particle size distribution of CSS18, CSS12, CSS6, C-18 and mCSS18 NPs. (E) Typical images of CSS18 (1), CSS12 (2), CSS6 (3), C-18 (4), mCSS18 (5) NPs with concentration of 1.5 mg Pt/mL and CSS18 NPs at 3 mg Pt/mL (6). (F) Tyndall Effect occurred in Pt(IV) NPs prepared with nanoprecipitation method: CSS18 (1), CSS12 (2), CSS6 (3), C-18 (4), mCSS18 (5).

mL carboplatin, CSS6, CSS12, CSS18, C-18 and mCSS18 NPs (or prodrugs) for 1 or 4 h. Ultimately, cells were dissociated and digested overnight for Pt detection by ICP-MS. And cells quantitation were carried out by BCA protein assay kit (Neobioscience Technology Co, Ltd.).

2.8. Cytotoxicity assay

The *In vitro* Cytotoxicity of all Pt(IV) NPs against 4T1, B16-F10, A2780 and LO2 cells were assessed by MTT assay. Typically, 4T1, B16-F10 and A2780 cells were seeded in 96-well plates at a density of 2 × 10^3 cells/well (3 × 10^3 cells/well for LO2) for 12 h, followed by treatment with serial dilution of CSS6, CSS12, CSS18, C-18, mCSS18 NPs and free carboplatin. The cells and preparations were further co-incubated for 48 h prior to the addition of 20 μl MTT solution (5 mg/mL). After another 4 h incubation, cells were washed with PBS and 200 μl DMSO was added for evaluation of cell viability by microplate reader at 490 nm.

2.9. DNA-Pt adduct

4T1 cells were cultured as above-mentioned in 6-well plates for 24 h, then 100 μM Pt equivalence of different nanossemblies were added. After 12 h incubation, the nucleus DNA of cells were extracted by mammalian genomic DNA extraction kit (NEST Biotechnology) and digested with nitric acid at 80 °C overnight. The Pt content was determined by ICP-MS.

2.10. Animals

All animals in this research were supplied by the Laboratory Animal Center of Shenyang Pharmaceutical University (Shenyang, Liaoning, China). All associated animal experiments were carried out according to the *Guidelines for the Care and Use of Laboratory Animals* approved by the Institutional Animal Ethical Care Committee (IAEC)ofShenyang Pharmaceutical University.

2.11. In vivo pharmacokinetic

Male Sprague − Dawley rats (200–250 g) were used to evaluate the pharmacokinetic profiles of Pt(IV) NPs. Prior to the experiments, the rats were fasted for 12 h. The animals were intravenously administered carboplatin solution, CSS6, CSS12, CSS18, C-18 and mCSS18 NPs at 3 mg Pt/kg (n = 5 for each group). At the predetermined time points (15 min, 1, 4, 8, 12 h), blood samples were collected and then centrifuged to obtain the plasma. Nitric acid (HNO_3, 65%, suprapure) was added into the plasma and allowed them to digest overnight. Then Pt content were measured by ICP-MS.

2.12. In vivo biodistribution

The *in vivo* distribution profiles of Pt(IV) NPs into tumor and other organs were assessed in 4T1 tumor-bearing Balb/c mice (female, n = 3). Mice with subcutaneous tumors of approximate 300 mm^3 were subjected to tail vein injection of carboplatin solution, CSS6, CSS12, CSS18, C-18 and mCSS18 NPs at 5 mg Pt/kg. At 4 and 12 h after dosing, mice were euthanized followed by the organs (heart, liver, spleen, lung and kidney) and tumors harvested. Then organs and tumors were washed in the saline, weighted and sheared by a tissue homogenizer. Then the tissue homogenates were digested by nitric acid (HNO_3, 65%, suprapure) overnight. Pt content in tissues and tumors were analyzed by ICP-MS.

2.13. In vivo antitumor efficacy

The female Balb/c mice model bearing 4T1 breast xenograft tumors were applied to investigate the *in vivo* antitumor efficacy. All mice were separated into seven groups (n = 5) randomly and inoculated with the same batch of 4T1 cells (5×10^6 cells per 100 μl). Mice with tumor volume of about 100 mm^3 were intravenously injected with 5% glucose, carboplatin dissolved with 5% glucose, CSS6, CSS12, CSS18, C-18 and mCSS18 NPs at 5 mg Pt/kg body weight every other day with total 4 times injection. The tumor size, 0.5 × (long side) × $(\text{short side})^2$, and body weight change of every mouse were recorded. After tumor monitoring, all mice were euthanized and their blood samples were collected for hepatorenal function test (ALT, alanine aminotransferase; AST, aspartate aminotransferase; BUN, Blood Urea Nitrogen and CREA, Creatinine), tissues (heart, liver, spleen, lung, and kidney) separated for H&E staining. B16-F10 xenograft tumor model in C57BL/6 female mice was also established which underwent the same dosing regimen. Tumor size and body weight of each mouse were also monitored every other day. When tumor volume was up to 2000 mm^3, diseased mice were considered as dying from excessive tumor burden and subjected to euthanasia.

Table 1
Characterization of Pt(IV) NPs (0.5 mg Pt/mL) determined by dynamic light scattering (DLS).

Pt(IV) NPs	Size (nm)	PDI	Zeta (mV)
CSS6	150.4 ± 21.53	0.409 ± 0.030	−19.1 ± 1.501
CSS12	102.4 ± 3.108	0.113 ± 0.033	−25.4 ± 1.992
CSS18	84.39 ± 1.054	0.132 ± 0.022	–22.5 ± 1.768
C-18	87.53 ± 4.805	0.193 ± 0.032	−29.7 ± 2.326
mCSS18	117.3 ± 4.513	0.290 ± 0.024	−14.6 ± 1.147

2.14. Statistical analysis

All the quantitative data are described using the mean ± SD (standard deviations), and statistical analysis was performed with Student's *t*-test and one-way ANOVA. $p < 0.05$ was considered statistically significant (* $p < 0.05$, ** $p < 0.01$, *** $p < 0.001$.).

3. Results and discussion

3.1. Synthesis of Pt(IV) prodrugs

We developed various carboplatin prodrugs with different axial disulfide-based ligands with synthetic routes shown in Fig. 2A. Both axial orientations of platinum atom were modified by symmetrical disulfide bond-inserted aliphatic chains that differs from each other in carbon chain length (CSS6. CSS12 and CSS18). No disulfide inserted Pt (IV) prodrug (C-18) and asymmetrically monoaxial carboplatin prodrug (mCSS18) were also prepared. The detailed synthetic approaches of all these amphiphilic Pt(IV) compounds were shown in Support Information. The precise structure of Pt(IV) prodrugs were confirmed by MS and ^1H NMR as shown in Figure S1-S5.

3.2. Self-stabilization of Pt(IV) NPs

Pt(IV) nanoparticles were fabricated with nanoprecipitation we previously reported (Yang et al., 2020; Sun et al., 2019). Typical images of all NPs showed spherical morphology in Fig. 2B and S6A-C. As shown in Table 1 and Fig. 2D, contrary to free carboplatin (Car), all amphiphilic Pt(IV) conjugates are able to assemble in H_2O at the concentration of 0.5 mg Pt/mL. Beyond the similar assembly behavior, the size and PDI of nanoparticles differ a lot, exhibiting an evident correlation to chain length of Pt(IV) conjugates: CSS18 ≈ C-18 < CSS12 < CSS6. Compared with CSS18, larger particle size and increased PDI of monoaxial mCSS18 was observed as well (CSS18 < mCSS18). When coming to Pt(IV) NPs at 1 mg Pt/mL and 1.5 mg Pt/mL, the relevance between nanoparticle properties and length of aliphatic branches was more evident (Table S1). Even precipitation occurred in the preparation process of CSS6 and mCSS18 NPs at 1.5 mg Pt/mL while CSS18 NPs at 6 mg Pt/mL showed uniform and transparent appearance, which is shown in Fig. 2E. In Fig. 2F, Tyndall Effect was confirmed in all nanoparticles at 1.5 mg Pt/mL by a laser beam except for CSS6 NPs, in which the white precipitation presented at the bottom of vial. It could be concluded that CSS6 NPs are incapable of stabilization at high concentration by the evidence of largest particle size and highest PDI. As for mCSS18 NPs, dim light beam was visible in supernatant but precipitation still existed, which indicates poor stability and weak assembly property. Of all nanoparticles, CSS18 had the best physicochemical properties and even stabilized at 1.5 mg Pt/mL with light blue and limpid outlook (Fig. 2C). These results suggest aliphatic chain length and location play a crucial role on self-stabilized manner of carboplatin prodrugs. Double axial and long lipid branches impart better assembly performance to Pt(IV) prodrugs than monoaxial and short branched ones. It could be also reasonably hypothesized that enough hydrophobicity of Pt(IV) amphiphiles contributes to NP integrity that might prevent prodrug against cleavage or attack in the blood circulation.

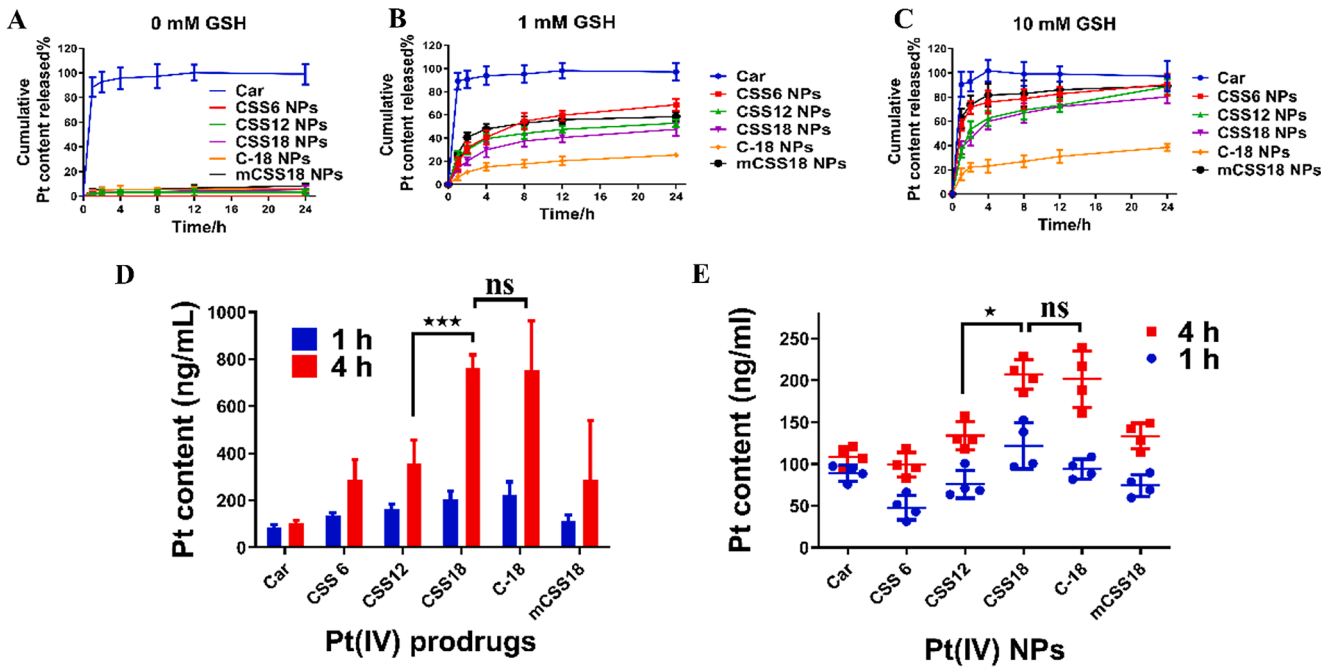

Fig. 3. Cumulative Pt release profiles of different formulations determined by ICP-MS in 10 mM PBS containing 0 mM (A), 1 mM (B) and 10 mM GSH (C). Cell uptake and intracellular drug accumulation of prodrug Car, CSS6, CSS12, CSS18, C-18, mCSS18 NPs (D) and their NPs (E) in 4 T1 cells which were determined by ICP-MS. (*$p < 0.05$, ** $p < 0.01$, *** $p < 0.001$, n = 3).

3.3. Colloidal stability

The stability of nanoparticles is of great significance to its manufacture, storage and clinical applications. As illustrated in Figure S7A and B, all NPs remained stable in size and PDI in 10 mM PBS 7.4 for one week except that CSS6 NPs has a sharp increase in particle size and PDI, which suggests uncertainty in stabilization control of nanoparticles composed of short lipid chain Pt(IV) amphiphiles. And facing chemical challenges from plasma proteins, which is simulated by 10% FBS, C-18, CSS12 and CSS18 NPs remained stable for 48 h with no visible appearance change and size fluctuation. CSS6 NPs and single aliphatic chain prodrug, mCSS18 NPs, showed poor stability with increased particle size at 48 h. In concert with assembly manner assay, precipitations were observed in CSS6 and mCSS18 NPs group even at low concentration (0.5 mg Pt/mL). Size growth, PDI increase and precipitation present in incubation media might indicated unsatisfactory property of short lipid chain Pt(IV) NPs when interacted with endogenous proteins.

3.4. In vitro drug release

As reported, the average reduced GSH level is about 1–11 mM in the cytoplasm which is much higher than that about 2–10 μM in the blood circulation and extracellular environment (Schafer and Buettner, 2001; Brülisauer et al., 2014). The redox potential preserved by intracellular GSH/GSSG (~-250 mV) is also much higher than the extracellular one (~-140 mV) and GSH/GSSH potential gap across cell membrane is broader than other thiol redox couples such as Cys/Cyss (Brülisauer et al., 2014; Moriarty-Craige and Jones, 2004). Disulfide bond is easy to be attacked or reduced by hydrophilic GSH via with thiol–disulfide exchange reaction which happens in the endogenous proteins to stabilize or deconstruct its tertiary and quaternary structures. To picture release profile of disulfide inserted Pt(IV) NPs, 10 mM GSH was used in the *in vitro* release assay to simulate reduction potential of tumor site. As illustrated in Fig. 3A, redox-sensitive NPs (CSS6, CSS12, CSS18 and mCSS18 NPs) showed accelerated Pt release of initial 70% at 4 h and final 80% at 24 h, which exceed over non-disulfide C-18 NPs at any time point. For release behavior of redox-sensitive NPs in 1 mM GSH buffer, the boosted release tendency over C-18 NPs was mitigated and final release percent of all groups was lower than that of 10 mM GSH (Fig. 3A-C). And C-18 NPs release just 25% platinum content in total after 24 h incubation in 1 mM GSH (Fig. 3B). Carboplatin solution reached diffusion balance quickly with > 90% released Pt content at 1 h in all mediums. While accumulate release was less than 10% of each group in 0 mM GSH buffer. With GSH level dependent release manners, it is reasonably speculated that disulfide bond guided prodrug nanoassemblies are much more GSH-sensitive than ordinary lipid-Pt(IV) prodrug and might be applied for rational design of cargo delivery with tumor selective response due to evaluated GSH level in tumor site. According to foregoing results, the longest aliphatic branched prodrug CSS18 with favorable self-stabilized behavior and good colloid stability, displayed basically equal GSH responsive capacity to other disulfide prodrugs. This enlightened that chemical structure adjustment of disulfide-tethered carboplatin(IV) molecules to enable enhanced assembly and stability dose not impair specific responsiveness triggered by intracellular GSH.

3.5. Intracellular Pt accumulation

The internalization of carboplatin is conducted mainly via copper influx transporter (CTR1) and organic cation transporter 2 (OCT2) (Holzer et al., 2011). Chemical modulation of Pt compound is reported to be likely to change the pathway of entry into cells (Chen et al., 2018). Axial aliphatic branched modification seem to make Pt(IV) molecules more prone to pass through lipid bilayer and enter cells with high intracellular accumulation (Ling et al., 2019; Li et al., 2018). The entry pathway of nanoparticles into cells is considered to be endocytosis mediated by functional proteins which differs from free molecules. With high Pt loading efficiency, nanoasemblies were expected to elevate platinum uptake which was investigated by cell uptake assay. As shown in Fig. 3D, intracellular drug accumulation of CSS18 and C-18 was higher than any other prodrug at 4 h but there were no significant differences between all prodrugs in 1 h. Strategy of prolonging axial lipid chain to regulate affinity with biofilm enhanced Pt(IV) complexes cellular uptake as widely reported. CSS18 or C-18 may be more likely to

Table 2
IC50 value (μM) of different Pt formulations treating for 48 h in 4 T1, B16, A2780, and LO2 cells.

Sample	4 T1	B16-F10	A2780	LO2
Car sol	24.37	2.242	206.5	47.28
CSS6 NPs	818.1	155.6	>1000	684.7
CSS12 NPs	34.37	1.882	35.62	76.95
CSS18 NPs	10.62	2.624	8.875	191.2
C-18 NPs	115.9	47.28	403.2	439.4
mCSS18 NPs	62.42	28.62	186.5	321.4

be inserted into the phospholipid bilayer due to the similar amphiphilic structure and even become component of cell membrane. It might make prodrug CSS18 or C-18 easy to sneak into cytoplasm via component exchange between membrane and cytosol. It is interesting that CSS18 NPs displayed the highest Pt uptake as well which is shown in Fig. 3E. PEGylated nano-formulations are generally believed to form hydration shell to cover chemical diversity of components when getting in touchwith surface phospholipid layer. The high intracellular Pt content detected of CSS18 NPs might derive from excellent stability in 1640 medium. While short chain branched CSS6 and mCSS18 NPs were inclined to be precipitated before being internalized by cells owing to initial larger size and lack of good stabilization.

3.6. In vitro cytotoxicity assay

Inspired by accelerated release and enhanced internalization of long branches octahedrally coordinated Pt(IV) prodrug NPs, *in vitro* antitumor efficiency was examined on different cell lines. IC50 values were listed in the Table 2 and Pt concentration dependent cytotoxicity curves of 4T1, B16-F10, A2780 and LO2 cells were shown in Figure S8A-D. CSS6 NPs showed the weakest inhibition against all cell lines than any other group, which had still inferior activity to non-sensitive C-18 NPs. Of all self-stabilized nanoparticles, CSS18 NPs exhibited the most powerful cytotoxicity in three cancer cell lines and even showed a close IC50 with carboplatin solution, implying long lipid branched tactics to deliver Car could gain antiproliferation benefits from elevated cellular Pt internalization and fast drug release mediated by disulfide bond. It deserved to be mentioned that all Pt(IV) NPs showed less potent cytotoxicity than free Car after 48 h incubation in LO2 cells, which makes it possible for this GSH-responsive Pt(IV)-lipid prodrug strategies to achieve tumor selectivity and low toxic (or harmless) in normal tissues.

3.7. Detection of nucleus DNA-Pt adduct

DNA is confirmed to be the major cellular target of platinum drugs where adducts and crosslinks are generated to impair its normal functions and further initiate apoptosis. As shown in Fig. 4A, Pt content of DNA extracted from 4T1 cells after incubation with Pt(IV) NPs was detected by ICP-MS. The overall amounts of adducts caused by double axial chain linked prodrugs are still associated with chain length: CSS18 > CSS12 > CSS6 NPs. Despite high intracellular accumulation, non-sensitive C-18 NPs had the lowest DNA-Pt adduct level probably because of difficulty in releasing carboplatin rapidly and thus delayed entry into nucleus or other DNA located organelle. While disulfide bond linked nanoparticles rendered more adducts detected by ICP-MS, suggesting rapid release of active Pt(II) molecules make great contributions to efficiency of coordination with DNA. Among them, CSS18 NPs with compelling stability in extracellular medium and swift Car release triggered by intracellular GSH, remained the most pronounced DNA adduct

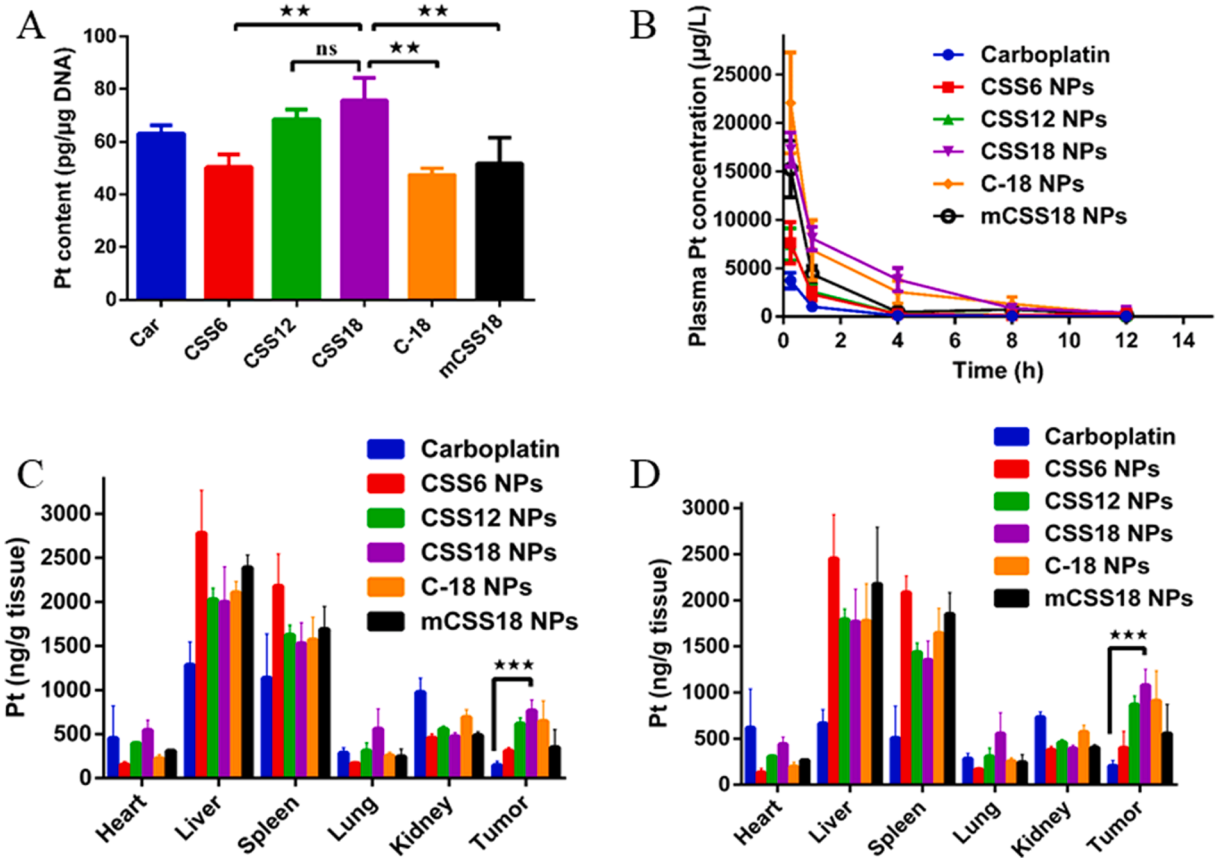

Fig. 4. (A) DNA binding Pt content in 4 T1 cells treated with carboplatin, CSS6, CSS12, CSS18, C-18, mCSS18 NPs for 12 h. (B) Mean plasma Pt concentration–time profiles of carboplatin, CSS6, CSS12, CSS18, C-18, mCSS18 NPs after i.v. administration in SD rats and biodistribution in 4 T1 tumor-bearing Balb/c mice (n = 3) at 4 h (C) and 12 h (D) (ns: no significant difference; *$p < 0.05$, **$p < 0.01$, ***$p < 0.001$, n = 3).

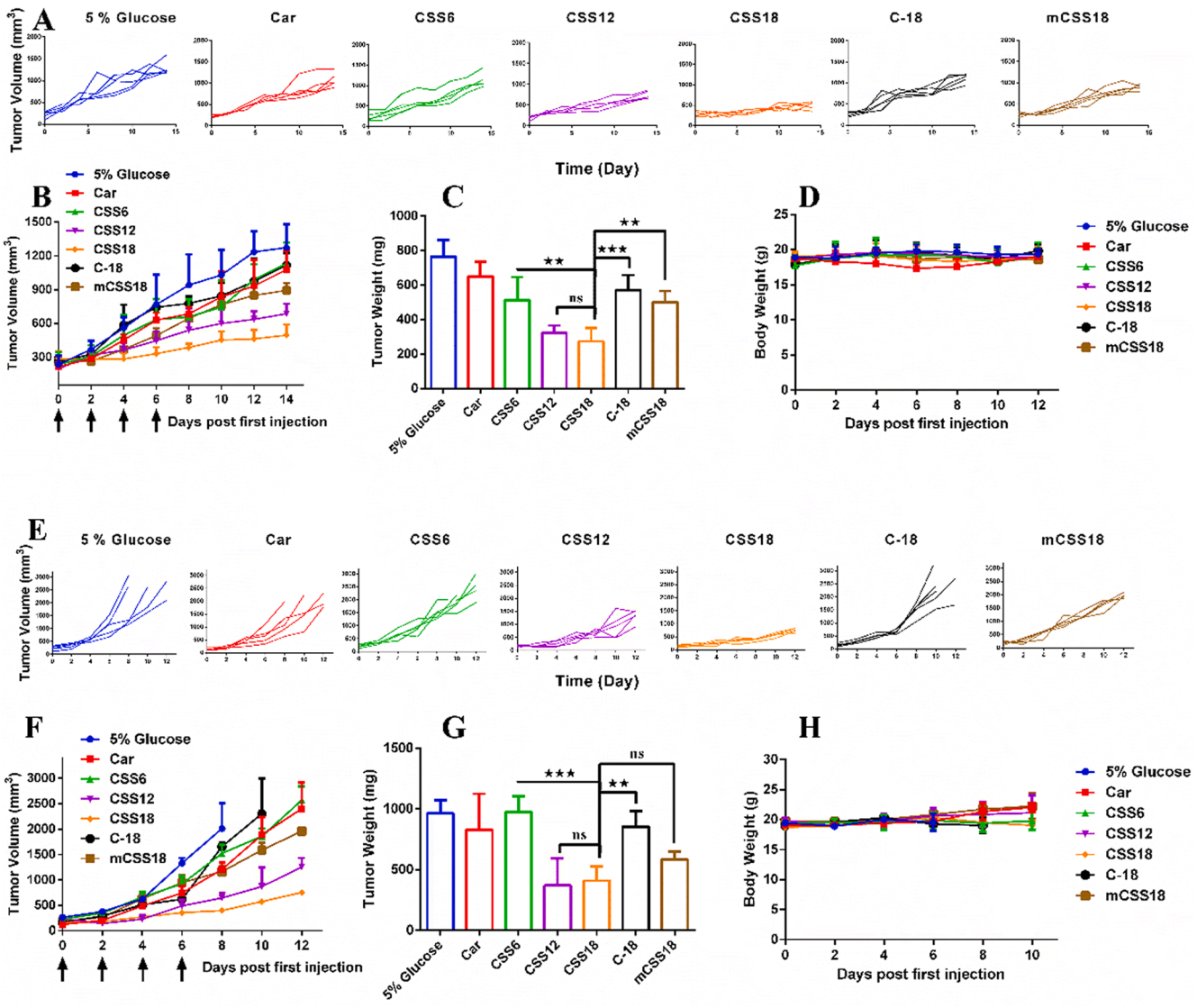

Fig. 5. The antitumor efficacy *in vivo*. (A) Tumor growth curve of each mouse from different groups of 4 T1 tumor-bearing Balb/c mice during treatment of 5% glucose, carboplatin solution, CSS6, CSS12, CSS18, C-18 and mCSS18 NPs (n = 5). The total tumor volume (B), tumor burden (C) and body weight (D) of 4 T1 tumor-bearing Balb/c mice (n = 5). (E) Tumor growth curve of each mouse from different groups of B16-F10 tumor-bearing C57BL/6 mice during therapy (n = 5). The total tumor volume (F), tumor burden (G) and body weight (H) of B16-F10 tumor-bearing C57BL/6 mice (n = 5). The arrow indicates the day of dosing different formulation via tail vein injection. (ns means no significant difference; $^{*}p < 0.05$, $^{**}p < 0.01$, $^{***}p < 0.001$, n = 5).

level. High DNA binding efficiency may be one of the most important factors that lead to cytotoxicity of CSS18 NPs.

3.8. *In vivo* pharmacokinetic

Colloid stability of prodrug was tested by co-incubation with 10% FBS and relatively long aliphatic chain grafted NPs (CSS12, CSS18 and C-18 NPs) showed good stability *in vitro*. Herein we further investigated the *in vivo* pharmacokinetic profiles of all Pt(IV) NPs in SD rats. As shown in Fig. 4B and Table S2, CSS18 and C-18 NPs had the most evident improved AUC of 36.11 mg·h·L^{-1} which was about 8-fold higher value than that of free Car. However, CSS6 NPs showed rapid elimination in plasma with just a little increased AUC (2.2-fold) and $t_{1/2}$ in comparison with Car. The overall prolonged circulation time and augmented AUC benefited from pharmacokinetic manners of different groups were ranked as: CSS18 ≈ C-18 > CSS12 ≈ mCSS18 > CSS6, which is inspiringly consistent with the order of carbon chain length grafted in the axis of platinum atom. It revealed that appropriate modification of amphiphilic Pt(IV) prodrug give rise to favorable *in vivo* fate of its nanoassemblies. It also verify our assumptions that enough hydrophobicity of Pt(IV) amphiphiles might preclude them from cleavage or attack in the blood circulation.

3.9. *In vivo* biodistribution

The biodistribution of five kinds of prodrug and free carboplatin in 4T1 bearing Balb/c mice model was also detected by ICP-MS. As illustrated in Fig. 4C and D, intravenous injected carboplatin was quickly eliminated in plasma compared with Pt(IV) NPs, exhibiting enriched distribution in kidney probably because of high hydrophilicity. As a primary organ vulnerable to platinum, renal toxicity is common during Pt treatment in clinic. Unlike free Car, all Pt(IV) NPs showed decreased Pt content in kidney, indicating an alleviated toxicity profile. While Pt (IV) NPs mainly accumulated in liver and spleen after intravenous administration due to elimination by reticuloendothelial system (RES). Notably, all NPs especially CSS18 and C-18 nanoparticles were more enriched in tumor site, attributable to enhanced permeability and retention (EPR) effect. With the most prolonged Pt residence in plasma

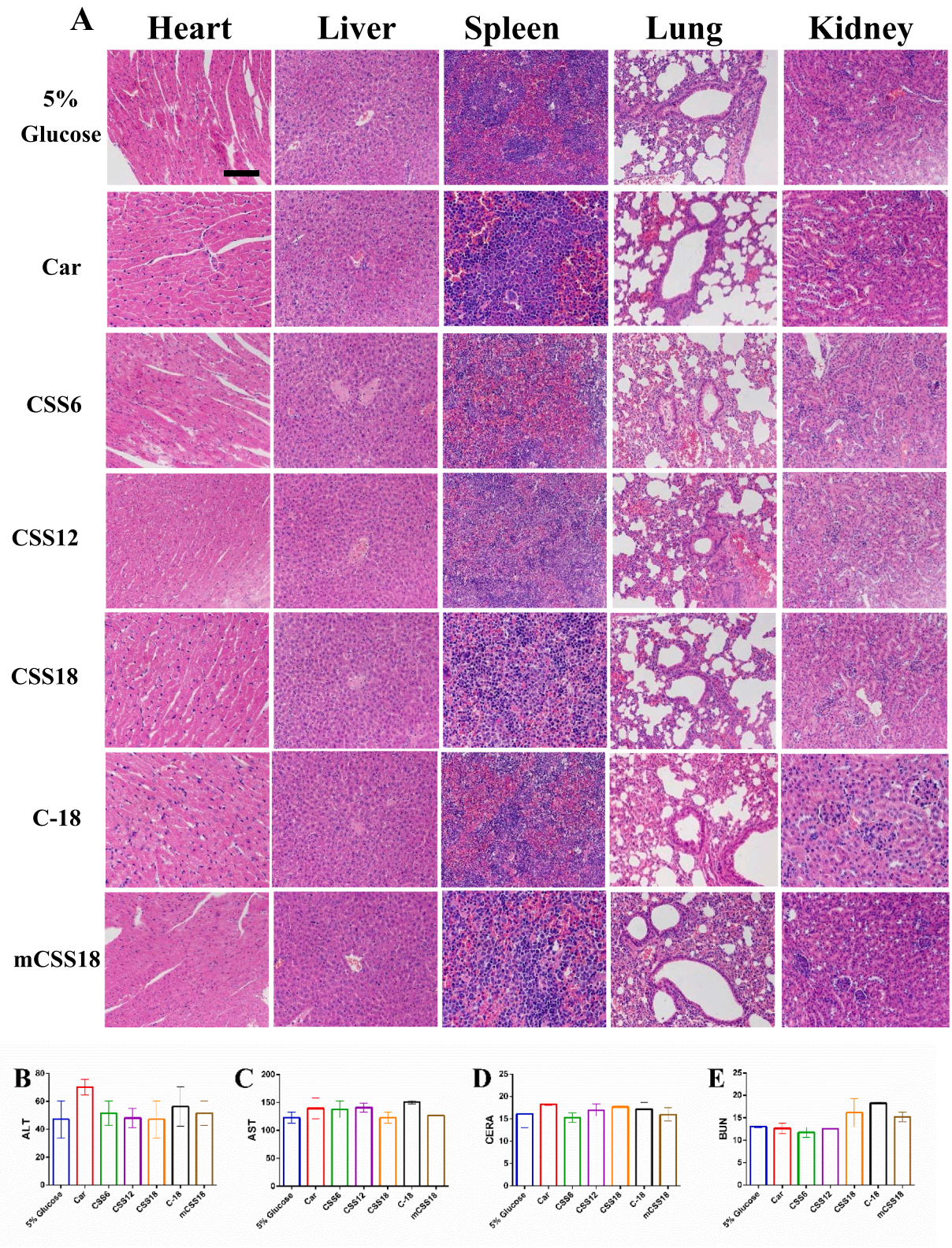

Fig. 6. Histopathological section (H&E staining) of the hearts, livers, spleens, lungs and tumors of Balb/c mice after different formulations administration. scale bar: 100 μm. Liver (ALT (B), AST (C)) and kidney (CERA (D), BUN (E)) functional parameters at day 14 after mice were sacrificed.

according to pharmacokinetics, CSS18 NPs exhibited maximal drug concentration detected in tumor with around 5-fold level of Car group. As a prerequisite for implementation of tumor selectivity and anti-proliferation efficiency, ideal pharmacokinetic behaviors make it possible for enhanced tumor accumulation.

3.10. In vivo antitumor efficacy

To evaluate the therapeutic effect of solid tumor, we investigated the efficacy of Pt(IV) NPs using 4T1 and B16-F10 xenograft model developed by subcutaneous inoculation of cancer cells. As illustrated in

Fig. 5A-C, 4T1 bearing Balb/c mice injected with 5% glucose loaded the largest tumor of about 1200 mm^3. Both CSS6 and C-18 NPs showed limited inhibition on tumor growth rate comparable to carboplatin solution, which was due to poor stability *in vivo* and delayed release of Pt chemotherapeutics, respectively. Mice receiving CSS18, CSS12 and mCSS18 NPs developed tumors with restrained growth rate and markedly inhibited volume (400, 700 and 900 mm^3) at day 14, especially CSS18 NPs enabling the slowest proliferation rate and the smallest tumor volume. Fig. 5D showed carboplatin-induced weight loss (>20%) at day 6, implying systemic toxicity occurred and resulted from nonspecific distribution of platinum. While the self-stabilized NPs treated groups exhibited negligible body weight changes and no other obvious toxic signs. For consideration of therapeutic universality, a much highly proliferative type, B16-F10 xenograft model in C57BL/6 mice, was used to evaluate antitumor efficiency of all formulations. Fig. 5E and F revealed a sharply increased tumor volume in mice receiving 5% glucose, hitting 2060 mm^3 at day 8. C-18 NPs treated groups follow the rapid enlargement tendency and reach an average tumor burden of 2302 mm^3, suggesting an inadequate efficacy of non-sensitive Pt(IV) prodrug. Other groups had significantly distinguished tumor volumes with no more than 2000 mm^3 at day 12. Tumor weight of each group showed consistent tendency to volume in Fig. 5G. The B16-F10 proliferation inhibition effect of all was determined as: CSS18 > CSS12 > mCSS18 > CSS6 ≈ Car > C-18 > 5% Glucose, which is basically in concert with inhibition outcome in 4 T1 model (CSS18 > CSS12 > mCSS18 > CSS6 ≈ Car ≈ C-18 > 5% Glucose). No weight loss was observed of all mice and even a few put on weight before euthanasia as shown in Fig. 5H, indicating no systemic toxicity. In particular, C-18 prodrug showed comparable self-stabilization capacity and plasma stability to CSS18 but had minimal antiproliferation effect of all assembled NPs which was as weak as carboplatin. These results verify that disulfide bond, as an essential linker of Pt(IV) prodrugs in this research, endows these nanoassemblies with reduction-sensitive character activated by intracellular GSH and thus, has superior antitumor performance to non-sensitive linkage. On the basis of the above facts, we are astonished to discover that a subtle relationship between carbon chain length of disulfide-inserted prodrugs and overall cancer therapeutic outcome is established: CSS18 > CSS12 > mCSS18 (equivalent to CSS9) > CSS6. As shown in Fig. 6A-D, no dysfunction was observed in H&E staining pictures of all groups and no noticeable abnormal values were found in hepatorenal function assay.

4. Conclusion

To sum up, a series of GSH-sensitive Pt(IV)-lipid conjugates were developed to build self-stabilized nanocarriers, in which disulfide bond act as a key intersection of hydrophilic carboplatin and aliphatic chains with different length. Double grafted and long axial lipid chain made Pt (IV) prodrugs more amphiphilic to be capable of self-stabilization like "special micelles". As branched aliphatic chains lengthen moderately, Pt (IV) prodrugs are characterized with good assembly stability, prolonged blood circulation and even enhanced cellular internalization. Benefiting from rapid Pt release triggered by GSH, insertion of disulfide bond endows Pt(IV) NPs with high cytotoxicity and anticancer activity. With rational design of chemical structure, CSS18 as the optimal prodrug candidate, exhibited good self-stabilized property and favorable stability in physiological environment which enabled sufficient Pt accumulation on tumor site. Duo to distribution discrepancy of intracellular and extracellular GSH, the initial release of carboplatin from CSS18 is negligible while these prodrug molecules are transformed into cytotoxic agents after internalization by cells. For comprehensive consideration of these results, the overall anticancer performance of Pt(IV) prodrugs showed a hydrophobicity or branch length dependent manner: CSS18 > CSS12 > mCSS18 (CSS9) > CSS6 > C-18. Moreover, negligible systemic toxicity and immunotoxicity were observed, suggesting a good biocompatibility of Pt(IV)-SS-lipid amphiphiles. These provide new insights into structure–activity relationship of Pt(IV) prodrug and open a new path to biosafety chemotherapeutic nanocarriers.

Declaration of Competing Interest

The authors declare that they have no known competing financial interests or personal relationships that could have appeared to influence the work reported in this paper.

Acknowledgement

This research was supported by the Career Development Program for Young and Middle-aged Teachers in Shenyang Pharmaceutical University (Shenyang, China). This research was also supported by Suzhou Science and Technology Development Project (SYSD2019171) and High-tech zone health talents key talent category (No.2019).

Appendix A. Supplementary material

Supplementary data to this article can be found online at https://doi.org/10.1016/j.ijpharm.2021.120923.

References

Rottenberg, S., Disler, C., Perego, P., 2021. The rediscovery of platinum-based cancer therapy[J]. Nat. Rev. Can. 21 (1), 37–50.
Wang, D., Lippard, S.J., 2005. Cellular processing of platinum anticancer drugs[J]. Nat. Rev. Drug. Discov. 4 (4), 307–320.
Zajac, J., Novohradsky, V., Markova, L., Brabec, V., Kasparkova, J., 2020. Platinum (IV) derivatives with cinnamate axial ligands as potent agents against both differentiated and tumorigenic cancer stem rhabdomyosarcoma cells[J]. Angew Chem. Int. Ed. Engl. 59 (8), 3329–3335.
Wang, X., Wang, X., Jin, S., Muhammad, N., Guo, Z., 2019. Stimuli-responsive therapeutic metallodrugs[J]. Chem. Rev. 119 (2), 1138–1192.
Rabik, C.A., Dolan, M.E., 2007. Molecular mechanisms of resistance and toxicity associated with platinating agents[J]. Can. Treat Rev. 33 (1), 9–23.
Hartmann, J.T., Lipp, H.-P., 2003. Toxicity of platinum compounds[J]. Expert. Opin. Pharmacother. 4 (6), 889–901.
Pan, Z.-Y., Tan, C.-P., Rao, L.-S., Zhang, H., Zheng, Y., Hao, L., Ji, L.-N., Mao, Z.-W., 2020. Recoding the cancer epigenome by intervening in metabolism and iron homeostasis with mitochondria-targeted rhenium(I) complexes[J]. Angew. Chem. Int. Ed. 59 (42), 18755–18762.
Doshi, G., Sonpavde, G., Sternberg, C.N., 2012. Clinical and pharmacokinetic evaluation of satraplatin[J]. Expert Opin. Drug Metab. Toxicol. 8 (1), 103–111.
Choy, H., Park, C., Yao, M., 2008. Current status and future prospects for satraplatin, an oral platinum analogue[J]. Clin. Cancer Res. 14 (6), 1633–1638.
Kelland, L., 2007. Broadening the clinical use of platinum drug-based chemotherapy with new analogues: satraplatin and picoplatin[J]. Expert Opin. Invest. Drugs 16 (7), 1009–1021.
Shi, J., Votruba, A.R., Farokhzad, O.C., Langer, R., 2010. Nanotechnology in drug delivery and tissue engineering: from discovery to applications[J]. Nano Lett 10 (9), 3223–3230.
Luo, C., Sun, J., Sun, B., He, Z., 2014. Prodrug-based nanoparticulate drug delivery strategies for cancer therapy[J]. Trends Pharmacol Sci 35 (11), 556–566.
Kuang, X., Chi, D., Li, J., et al. Disulfide bond based cascade reduction-responsive Pt(IV) nanoassemblies for improved anti-tumor efficiency and biosafety[J]. Colloids and Surfaces B: Biointerfaces, 2021, 203.
Wang, Y., Liu, D., Zheng, Q., et al., 2014. Disulfide bond bridge insertion turns hydrophobic anticancer prodrugs into self-assembled nanomedicines[J]. Nano Lett, 2014, 14(10): 5577–5583.
Yang, Y., Sun, B., Zuo, S., Li, X., Zhou, S., Li, L., Luo, C., Liu, H., Cheng, M., Wang, Y., Wang, S., He, Z., Sun, J., 2020. Trisulfide bond-mediated doxorubicin dimeric prodrug nanoassemblies with high drug loading, high self-assembly stability, and high tumor selectivity[J]. Sci. Adv. 6 (45), eabc1725. https://doi.org/10.1126/sciadv.abc1725.
Zuo, S., Sun, B., Yang, Y., Zhou, S., Zhang, Y.u., Guo, M., Sun, M., Luo, C., He, Z., Sun, J., 2020. Probing the superiority of diselenium bond on docetaxel dimeric prodrug nanoassemblies: small roles taking big responsibilities[J]. Small 16 (45), 2005039. https://doi.org/10.1002/smll.v16.4510.1002/smll.202005039.
Cheetham, A.G., Chakroun, R.W., Ma, W., Cui, H., 2017. Self-assembling prodrugs[J]. Chem. Soc. Rev. 46 (21), 6638–6663.
Chen, Q., Yang, Y., Lin, X., et al., 2018. Platinum(iv) prodrugs with long lipid chains for drug delivery and overcoming cisplatin resistance[J]. Chem. Commun. (Camb) 54 (42), 5369–5372.
Ling, X., Tu, J., Wang, J., Shajii, A., Kong, N.a., Feng, C., Zhang, Y.e., Yu, M., Xie, T., Bharwani, Z., Aljaeid, B.M., Shi, B., Tao, W., Farokhzad, O.C., 2019. Glutathione-responsive prodrug nanoparticles for effective drug delivery and cancer therapy[J]. ACS Nano 13 (1), 357–370.

Damle, N.K., Frost, P., 2003. Anti body-targeted chemotherapy with immunoconjugates of calicheamicin[J]. Curr. Opin. Pharmacol. 3 (4), 386–390.
Schafer, F.Q., Buettner, G.R., 2001. Redox environment of the cell as viewed through the redox state of the glutathione disulfide/glutathione couple[J]. Free Radic Biol Med 30 (11), 1191–1212.
Brülisauer, L., Gauthier, M.A., Leroux, J.-C., 2014. Disulfide-containing parenteral delivery systems and their redox-biological fate[J]. J. Control. Release 195, 147–154.
Sun, B., Luo, C., Yu, H., Zhang, X., Chen, Q., Yang, W., Wang, M., Kan, Q., Zhang, H., Wang, Y., He, Z., Sun, J., 2018. Disulfide bond-driven oxidation- and reduction-responsive prodrug nanoassemblies for cancer therapy[J]. Nano Lett 18 (6), 3643–3650.
Luo, C., Sun, J., Sun, B., Liu, D., Miao, L., Goodwin, T.J., Huang, L., He, Z., 2016. Facile fabrication of tumor redox-sensitive nanoassemblies of small-molecule oleate prodrug as potent chemotherapeutic nanomedicine[J]. Small 12 (46), 6353–6362.
Lee, M.H., Yang, Z., Lim, C.W., Lee, Y.H., Dongbang, S., Kang, C., Kim, J.S., 2013. Disulfide-cleavage-triggered chemosensors and their biological applications[J]. Chem. Rev. 113 (7), 5071–5109.
Reshetnikov, V., Daum, S., Janko, C., Karawacka, W., Tietze, R., Alexiou, C., Paryzhak, S., Dumych, T., Bilyy, R., Tripal, P., Schmid, B., Palmisano, R., Mokhir, A., 2018. ROS-responsive N-alkylaminoferrocenes for cancer-cell-specific targeting of mitochondria[J]. Angew. Chem. Int. Ed. Engl. 57 (37), 11943–11946.
Yang, G.-G., Pan, Z.-Y., Zhang, D.-Y., Cao, Q., Ji, L.-N., Mao, Z.-W., 2020. Precisely assembled nanoparticles against cisplatin resistance via cancer-specific targeting of mitochondria and imaging-guided chemo-photothermal therapy[J]. ACS Appl. Mater. Interfaces 12 (39), 43444–43455.
Wang, H., Xie, H., Wang, J., Wu, J., Ma, X., Li, L., Wei, X., Ling, Q.i., Song, P., Zhou, L., Xu, X., Zheng, S., 2015. Self-assembling prodrugs by precise programming of molecular structures that contribute distinct stability, pharmacokinetics, and antitumor efficacy[J]. Adv. Funct. Mater. 25 (31), 4956–4965.
Shi, Y., Van Der Meel, R., Theek, B., et al., 2015. Complete regression of xenograft tumors upon targeted delivery of paclitaxel via Pi-Pi stacking stabilized polymeric micelles [J]. ACS Nano 9 (4), 3740–3752.
Sun, B., Luo, C., Zhang, X., Guo, M., Sun, M., Yu, H., Chen, Q., Yang, W., Wang, M., Zuo, S., Chen, P., Kan, Q., Zhang, H., Wang, Y., He, Z., Sun, J., 2019. Probing the impact of sulfur/selenium/carbon linkages on prodrug nanoassemblies for cancer therapy[J]. Nat Commun 10 (1). https://doi.org/10.1038/s41467-019-11193-x.
Moriarty-Craige S E, Jones D P. EXTRACELLULAR THIOLS AND THIOL/DISULFIDE REDOX IN METABOLISM[J]. 2004, 24(1): 481-509.
Holzer A.K., Manorek, G.H., Howell, S.B., 2006. Contribution of the major copper influx transporter CTR1 to the cellular accumulation of cisplatin, carboplatin, and oxaliplatin[J]. Mol Pharmacol, 2006, 70(4): 1390-1394.
Lee, Y.-Y., Choi, C.H., Do, I.-G., Song, S.Y., Lee, W., Park, H.S., Song, T.J., Kim, M.K., Kim, T.-J., Lee, J.-W., Bae, D.-S., Kim, B.-G., 2011. Prognostic value of the copper transporters, CTR1 and CTR2, in patients with ovarian carcinoma receiving platinum-based chemotherapy[J]. Gynecol. Oncol. 122 (2), 361–365.
Li, T., Xiang, W., Li, F., Xu, H., 2018. Self-assembly regulated anticancer activity of platinum coordinated selenomethionine[J]. Biomaterials 157, 17–25.